High-temperature thermal conductivity of porous Al_2O_3 nanostructures

L. Braginsky*
Institute of Semiconductor Physics, 630090 Novosibirsk, Russia

V. Shklover
Laboratory of Crystallography, Swiss Federal Institute of Technology, CH-8092 Zurich, Switzerland

H. Hofmann and P. Bowen
Powder Technology Laboratory, Swiss Federal Institute of Technology, CH-1015 Lausanne, Switzerland
(Received 13 May 2004; published 5 October 2004)

The temperature dependence of the thermal conductivity of porous, nanostructured alumina has been measured. It is shown that this dependence can be described with a single parameter, the value of which depends on the intergrain boundary structure and is independent of the grain size and porosity.

DOI: 10.1103/PhysRevB.70.134201 PACS number(s): 65.80.+n, 63.22.+m, 68.65.−k, 44.30.+v

I. INTRODUCTION

The problem of heat transfer in ceramic nanostructures is important due to possible application of such materials as the thermal barrier coatings. The operation temperatures of ceramic coatings are about or exceed 1000 °C. There are two mechanisms that are important for the heat transport in nonmetallic solids at such temperatures: the phonon and radiative mechanisms. Nanostructuring is assumed to decrease the phonon or photon mean free path, and so decrease the thermal conductivity. Indeed, thermal conductivity of nanostructures can be reduced in comparison with its bulk value.[1]

Propagation of phonons is an important mechanism of heat transfer at high temperatures. Note that the temperature of 1000 °C exceeds the Debye temperature for most dielectrics. This means that the phonons whose wavelength is similar to the lattice constant are most important for the heat transport. The commonly used continuum approximation is not appropriate to consider the intergrain transport of these short-wavelength phonons. Indeed, to investigate this problem, the well-known boundary conditions are usually applied on the corresponding components of the elastic field (an elastic displacement and strength). These boundary conditions arise as a result of averaging of the elastic fields over some region at the interface. The size of this region in the normal-to-boundary direction should significantly exceed the lattice constant. This procedure is appropriate for long-wavelength phonons, but it is not appropriate for short-wavelength phonons whose wavelength is similar to the lattice constant and for which such averaging can not be done.

The structure of a grain boundary is very important with respect to its interaction with short-wavelength phonons. Ideally the position of each atom at the interface should be known. However, there is no reliable experimental data on the atomic arrangement of the interface. One may expect a disordered (amorphous) structure of the grain boundaries (or necks between the grains, observed during the first and second stage of the sintering procedure). This makes it difficult to propose a microscopic model of the grain boundaries. Moreover, this complicates investigation of thermal conductivity in terms of the lattice wave theory.[1] The model we have proposed[2] is free of these shortcomings. It considered the short-wavelength phonon transport in granular media as a phonon hopping between neighboring grains. A grain boundary is considered phenomenologically. The only parameter describing the interface structure is considered as an adjustable parameter. It could be calculated only if an atomistic model of the interface structure can be proposed.

The radiative component of the thermal conductivity was found to be significant at high temperatures ($T \gtrsim 1000$ °C).[1] The thickness of the ceramic layer of interest is in the range of some hundred micrometers to around a millimeter. For this reason it was assumed that the mean free path of photons is equal to the film thickness. This is a rough estimate of the radiative component in thin films; in particular, the influence of the structure disorder on the photon mean free path in thick films can also be important.

In this paper we report results of our studies on porous $\alpha-Al_2O_3$ nanostructures. The Debye temperature of this material is $T_D = 1042$ K. We prepared two sets of three $\alpha-Al_2O_3$ nanostructures each distinguished by the grain size, porosity, and grain boundary structure. The thermal conductivity (TC) of the structures is much lower than that of an Al_2O_3 single crystal. In addition, it does not show any significant temperature dependence. Such behavior of TC is characteristic for the bounded structures due to phonon confinement. It has been exhibited in numerical simulations for nanowires,[3] layered structures and superlattices with[4] and without[5] quantum dots, and has been observed in experiments.[6]

The model we have adopted takes into account both the phonon and radiative mechanisms of thermal conductivity. To consider the phonon transport in porous nanostructures we used the theory previously developed by the authors.[2] The pores in some of our samples are of the size comparable to the grain size. For this reason we use the percolation model[7] to improve our theoretical model[2] and render it applicable to nanostructured materials of high porosity.

The length of the electromagnetic waves radiated at $T \sim 1000$ °C significantly exceeds the lattice constant; this allows us to apply the continuum approximation to investigate the radiative component of the thermal conductivity. To de-

TABLE I. Experimental data used in calculation.

Sample	Sintering temperature (°C)	Holding time (min)	Grain size (nm)	Deviation of the grain size (%)	Porosity (%)	Pore size (nm)	Coordination number	Cohesion	Contact diameter (nm) measured	Contact diameter (nm) calculated[a]	Thickness (mm)	t
FD1/1	1050	0	174	36	43	300	6.45	0.65	93	103	1.205	0.069
FD1/2	1020	3	161	16	27	310	9.27	0.76	100	142	1.07	0.073
FD1/3	1040	0	360	16	3	570	12.1	>0.9	270	355	1.34	0.066
FD2/1	1050	1	270	20*[b]	37	280	7	0.53	250	155	1.57	0.028
FD2/2	1020	3	315	15*	25	200	8.92	0.53	280	245	1.69	0.038
FD2/3	1040	0	450	15*	7	350	12.1	>0.9	432	432	1.69	0.030

[a]Calculated after Skorohod Ref. 14.
[b]Symbol * marks the estimated values.

termine this component, we consider the electromagnetic wave propagation in a granular material.

II. EXPERIMENT

A. Sample preparation

Commercial high purity transition alumina powder (Baikowski CR125; samples FD1/1–FD1/3) as well as MgO doped (0.5 wt%) γ-alumina powder (Baikowski CR11325; samples FD2/1–FD2/3) were used. The powders were attrition milled for 3 h with dispersant addition, freeze-dried and cold isostatically pressed. The samples were consolidated by spark plasma sintering using a heating rate of 200 °C/min up to the sintering temperatures of 1400 °C and holding times ranging from 0 to 5 min. The pressure was applied from the beginning of the sintering cycle and released during cooling. These different sintering conditions were chosen to produce different microstructures (grain size, porosity) (Table I).

B. Characterization of the samples

The porosity, grain size as well as the contact area between the grains were determined using image analysis methods applied to SEM pictures of polished and thermally etched samples. Additionally TEM studies of the samples FD1/1, FD1/2, and FD1/3 sintered at different conditions (Fig. 1) were performed with TEM Philips CM300, operating at 300 kV. The samples were coated with carbon layer to avoid charging.

C. Thermal conductivity measurements

The laser flash method was used for measurements of heat diffusivity in a "TC-3000H/L SINKU-RIKO" device as described in Refs. 8 and 9.

III. THEORY

The two mechanisms important for the heat transport in nonmetallic solids at high (of the order of Debye or higher) temperatures are: the phonon and radiative mechanisms. The first one relates to the movement of atoms in the crystalline lattice; the second one is due to the electron transitions between the energy levels in these atoms. If we neglect the relation between the energy levels and spacing between the atoms, then both mechanisms can be considered independently. This assumption seems to be reasonable, if the amplitude of the atomic oscillation is considerably lower than the lattice constant. We can then write

$$\kappa = \kappa_{\mathrm{ph}} + \kappa_{\mathrm{r}},$$

where κ is the thermal conductivity, κ_{ph} and κ_{r} are its phonon and radiative components, and consider each of them separately.

A. Phonon contribution to thermal conductivity

To investigate the high temperature phonon transport in nanostructures we assume that two mechanisms are dominant: scattering at the grain boundaries and the phonon-phonon interaction. At the same time, for the materials whose thermal conductivity is considerably reduced due to nanostructuring the phonon scattering at the grain boundaries is of most importance. This scattering determines the phonon mean free path that becomes now comparable with the grain size and is independent of the phonon wavelength. This means that the phonons whose wavelength is of about the lattice constant determine the thermal conductivity at high temperatures. This distinguishes nanostructured materials from single crystals or amorphous ones where the phonons

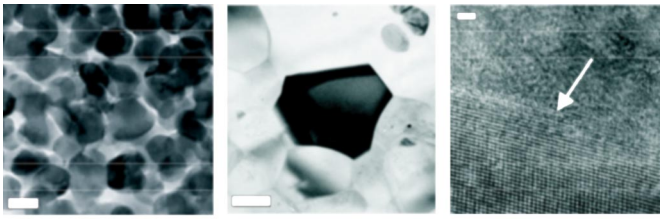

FIG. 1. TEM images. (a) Smaller grain size, lower density sample FD1/2, scale bar 200 nm. (b) Larger grain size, higher density sample FD1/3, scale bar 200 nm. (c) Two sintered grains in powder FD1/2. The interface (indicated with an arrow) has a thickness ~1 nm. Both grains are crystalline, but oriented differently and the crystalline fringes can be easily seen only on one of them. Scale bar 2 nm.

of different wavelength are of the same importance for TC.[1]

We adopt the following model. We start with the phonon states that initially were localized at the individual grains of the nanostructure and then consider their transport as the phonon hopping between the grains. This allows us to reduce the problem of the phonon transport to the problem of electrical conductivity of a net of arbitrary resistors R_{ij}, which correspond to relevant grain boundaries (between the i-th and j-th grains). This yields the following expression for TC:[2]

$$\kappa_{ph} = \frac{k_B^2 T Z t \bar{S} \Phi(\sigma)}{3\pi\hbar a^2 d} \int_0^{1/\theta} B(x)dx, \tag{1}$$

where

$$B(x) = \frac{9}{2}\theta^4 \frac{x^4 e^x}{(e^x-1)^2}\left(x - \frac{1}{\theta}\right)^2, \quad \theta = \frac{T}{T_D},$$

T is the temperature, T_D is the Debye temperature, $\hbar$ and k_B are the Planck and Boltzmann constants, a is the lattice constant, d is the grain size, $\bar{S}$ is the main area of the intergrain boundary (the "neck" size), and Z is the coordination number. Deviation of this parameters from its mean value is determined with the parameter of disorder Φ. It has been estimated in Ref. 2 as

$$\Phi = \left(1 + \frac{2\sigma^2}{Z}\right)^{-1}.$$

σ is the mean relative deviation of $\bar{S}$. Equation (1) results in the temperature dependence of TC that increases at $T < T_D$, and becomes constant at $T > T_D$. Thus, for $T > T_D$ Eq. (1) yields

$$\kappa_{ph} = \frac{k_B^2 Z t \bar{S} \Phi(\sigma) T_D}{20\pi\hbar a^2 d}. \tag{2}$$

The main difference between Eq. (1) from the one derived in Ref. 2 arises from the factor $Z/3\pi$. Indeed, in the absence of porosity the value of $Z\bar{S}$ is the total surface area of the grain and therefore it is a constant. In our experiments (Table I), however, it is not so because of complexity of the grain shape and porosity. The factor $Z/3\pi$ is valid if $Z \gg 1$. In particular, for $Z \sim 12$.[10]

To consider the phonon-phonon scattering we suppose that some additional resistors (the value of which is $r_i = \kappa_i d$, where κ_i is the bulk part of TC) are series connected to the boundary ones (R_{ij}). This leads to the following expression for TC:

$$\kappa_{ph} = k_B T \int_0^{1/\theta} \frac{\kappa_i B(x) Z t \bar{S} \Phi}{3\pi\hbar k_B^{-1} \kappa_i a^2 d + k_B T_D B(x) Z t \bar{S} \Phi} dx. \tag{3}$$

Here $\kappa_i = \kappa_i(T)$ is the thermal conductivity of the single crystal; an influence of impurities and other bulk mechanisms of phonon scattering can also be included in this value. It is important that all parameters of Eq. (3) except t can be measured experimentally. The t value describes interface transparency for the phonon hopping. To estimate it, the equations of movement for each atom at the interface have to be solved. We will not carry out this procedure, but we will consider the t value as an adjustable parameter. It depends only on the interface structure and is independent of the grain size and porosity. So, it should be similar for nanostructures prepared using the same technology. This fact will be tested experimentally in this paper.

B. Radiative part of thermal conductivity

A radiative contribution to the thermal conductivity arises from photon emission caused by electron transport. These photons can then be absorbed by the electrons. If the photon mean free path is considerably less than the size of the specimen, then the photon gas achieves a local thermodynamic equilibrium with the phonons. This allows us to consider the energy transport that is accompanied by the photons as a radiative component of thermal conductivity and estimate it as

$$\kappa_r = \frac{c}{3\sqrt{\varepsilon}} \int_0^\infty C_V(\omega) l(\omega) d\omega, \tag{4}$$

where c, ω, and $l(\omega)$ are the photon speed, frequency, and mean free path, ε is the dielectric permittivity,

$$C_V(\omega)d\omega = \frac{\hbar}{\pi^2 c^3}\frac{\partial}{\partial T}\left(\frac{\omega^3}{e^{\hbar\omega/k_B T}-1}\right)d\omega$$

is the heat capacity of the photons of the frequency ω.

Let us estimate the mean free path of the thermal photon $\hbar\omega \sim k_B T$ in a perfect $\alpha - Al_2O_3$ single crystal.

$$l(\omega) = \frac{c}{\sqrt{2\pi\omega\sigma}} \sim \frac{c}{\sqrt{2\pi N_e e^2/m^*}}, \tag{5}$$

where $\sigma = N_e e^2 \tau / m^*$ is the electric conductivity,[11] e and m^* are the charge and effective mass of the electron, τ is the electron relaxation time; at high temperatures it can be estimated as $\tau = \hbar/(k_B T)$, so that

$$\sigma = \frac{N_e e^2 \hbar}{m^* k_B T}.$$

N_e is the electron density. In a perfect crystal it can be estimated as

$$N_e = 2\left(\frac{2\pi m^* k_B T}{(2\pi\hbar)^2}\right)^{3/2} e^{-E_g/2k_B T}, \tag{6}$$

where for the band gap and effective mass values we have $E_g \approx 8.7$ eV, $m^* \approx 0.35 m_e$ (e and m_e are the charge and mass of the free electron).[12] Then

$$\kappa_r = \frac{k_B^4 T^3}{3\pi^2 c\hbar^3 \sqrt{2\pi N_e e^2/m^*}} \int_0^\infty \frac{x^4 dx}{\sqrt{x}(e^x-1)^2}. \tag{7}$$

Using Eqs. (5)–(7) for $T = 2000$ K yields $\kappa_r \approx 11$ W/(m K), and $l \approx 14$ cm. This means that a perfect Al_2O_3 crystal shows no resistance to the photon transport. The resistance could arise from the impurities or intrinsic defects (the energy level of the defect closest to the top of the valence band is E_i

$=0.3$ eV).[13] The latter can be responsible for heat resistance if their density is rather large, so that l becomes smaller than thickness of the specimen L. The effect can be estimated by Eq. (7), where $N_e \sim N_i e^{-E_i/k_B T}$ and m^* is effective mass of the hole, N_i is the defect density. However, this yields κ_r that is usually small, if $l \ll L$.

It is easy to understand the reason. The electron density is low at low temperature. This means long mean free paths both of electrons and photons [Eq. (5)]. Increase of the temperature leads to increase of the photon part of the heat capacity (which is proportional to T^3), but also to rapid decrease of the photon mean free path (which exponentially depends on temperature).

Appreciable contribution to the radiative component could originate from the electron levels localized less than 0.1 eV from a band edge. They can be the electrons from impurity or surface levels segregated from the conductive or valence bands (electrons from dangling bonds). In the latter case, the density of the levels can be roughly estimated as $N_i \lesssim 24p/(\pi a^2 D)$, where D is the pore size. Such levels become ionized at $T \gtrsim 1000\,^\circ$K. Then $N_e \to N_i$ becomes independent of temperature, so that κ_r increases as T^3.

Crystal disorder decreases the phonon mean free path and so decreases the radiative component. To estimate this effect we take into account that wavelength of the heat photons at $T=1000$ K is of about 5000 nm, so that it significantly exceeds the grain size. This allows us to use a continuum approximation: We consider the electromagnetic wave propagation in the media with the position dependant dielectric permittivity. In the first approximation (with respect to ratio of the grain size to the photon wavelength) this effectively change the permittivity, however, in the second approximation this leads to decay of the electromagnetic waves due to the structural disorder. The decay length considerably exceeds not only the grain size, but also the wavelength.

To consider the propagation of electromagnetic waves in a granular material we find the solution of the Maxwell equations in the media with the dielectric permittivity $\varepsilon(r)=\varepsilon+\xi(\mathbf{r})$, where ε is the average permittivity, which is independent of $\mathbf{r}$, and the random function $\xi(\mathbf{r})$ is its deviation. This allows us to express the electric and magnetic fields of the waves via the correlation function $W(\mathbf{r}-\mathbf{r}')=\langle \xi(\mathbf{r}')\xi(\mathbf{r})\rangle$, which we assume to be equal to $W(\mathbf{r}-\mathbf{r}')=\vartheta^2 \times \exp(-|\mathbf{r}-\mathbf{r}'|/\mathcal{R})$, where ϑ is the mean square deviation of the permittivity and $\mathcal{R} \simeq d$ is the correlation length. Unlike the commonly used Gauss correlation function, this one is more appropriate for the steplike random values ($\epsilon(\mathbf{r})=\epsilon_1=\epsilon$ in the grains or $\epsilon(\mathbf{r})=\epsilon_2=1$ in the pores).

We found that disorder leads to the effective correction to the permittivity $\tilde{\varepsilon}=\varepsilon-\vartheta^2/3\varepsilon$ and attenuation of the electromagnetic waves $\gamma \propto \omega^4 \mathcal{R}^3$ (see the Appendix for details of computations). The effective mean free path is

$$\frac{1}{l_{eff}} = \frac{1}{l(\omega)} + \frac{1}{l_{sc}(\omega)}, \quad \text{where} \quad l_{sc}(\omega) = \gamma^{-1} = 3\vartheta^{-2}\mathcal{R}^{-3}(\omega/c)^{-4}. \tag{8}$$

Here $\vartheta^2=p(1-p)(\epsilon-1)^2$, and p is the porosity.

The effective mean free path $l_{\text{eff}}(\omega)$ substitutes $l(\omega)$ in Eq. (4). It is apparent this is approximately the smallest value between $l(\omega) \propto \omega^{-1/2}$ and $l_{sc}(\omega) \propto \omega^{-4}$. In the perfect crystal $l(\omega) \ll l_{sc}(\omega)$, and the value of $\omega = k_B T/\hbar$ is effectively the upper limit for the integral (4). In the real crystal the solution ω_0 of the equation $l(\omega_0)=l_{sc}(\omega_0)$ can be either larger or smaller than $k_B T/\hbar$. In the first case the disorder has no appreciable influence on κ_r, in the second one the value of $\omega_0 < k_B T/\hbar$ becomes the effective upper limit of Eq. (4); this decreases the radiative component κ_r.

IV. RESULTS AND DISCUSSION

The results of the TEM study of our samples are presented in Fig. 1, where the structure of the interfaces between the $\alpha-Al_2O_3$ grains is shown. This is important, because it influences the phonon propagation in nanopowder. The TEM study shows, that

1. The interfaces between the $\alpha-Al_2O_3$ grains are very thin ($\sim$1 nm, Fig. 1)
2. No epitaxial relation between the neighboring crystalline $\alpha-Al_2O_3$ grains was observed.

Table I presents results of the structure measurements of our specimens together with the values of the parameter t for each of them. These values of t ensure the best fit of Eq. (3) with measured temperature dependence of TC (Fig. 3). The value of t does not vary significantly for the specimens of each set, but change approximately two times for the specimens of different sets. This means that the parameter t depends on the intergrain interface structure, but it is independent of the grain size and porosity.

To understand this, we recall that $\sim$0.5 wt % of MgO was added during the preparation of FD2/1–FD2/3. This amount is much larger than solubility of MgO in alumina, therefore most of the added MgO should be located at the grain boundaries affecting the t value.

Figure 2 presents results of our TC measurements for the FD1/2 specimen along with temperature dependence of Al_2O_3 thermal conductivity in the bulk that was measured in Ref. 15. It is apparent that our experimental dots do not show significant temperature dependence. In addition, TC of our structures is much less than that of the bulk single crystal;

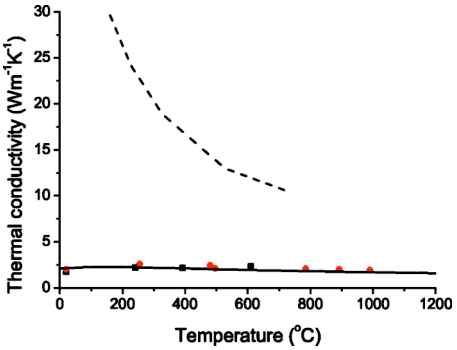

FIG. 2. (Color online) Temperature dependence of TC of the sample FD1/2: measured (dots) and calculated (solid line). Different types of the dots label the different series of the measurements. Dashed line indicates TC of the bulk Al_2O_3 single crystal (Ref. 15).

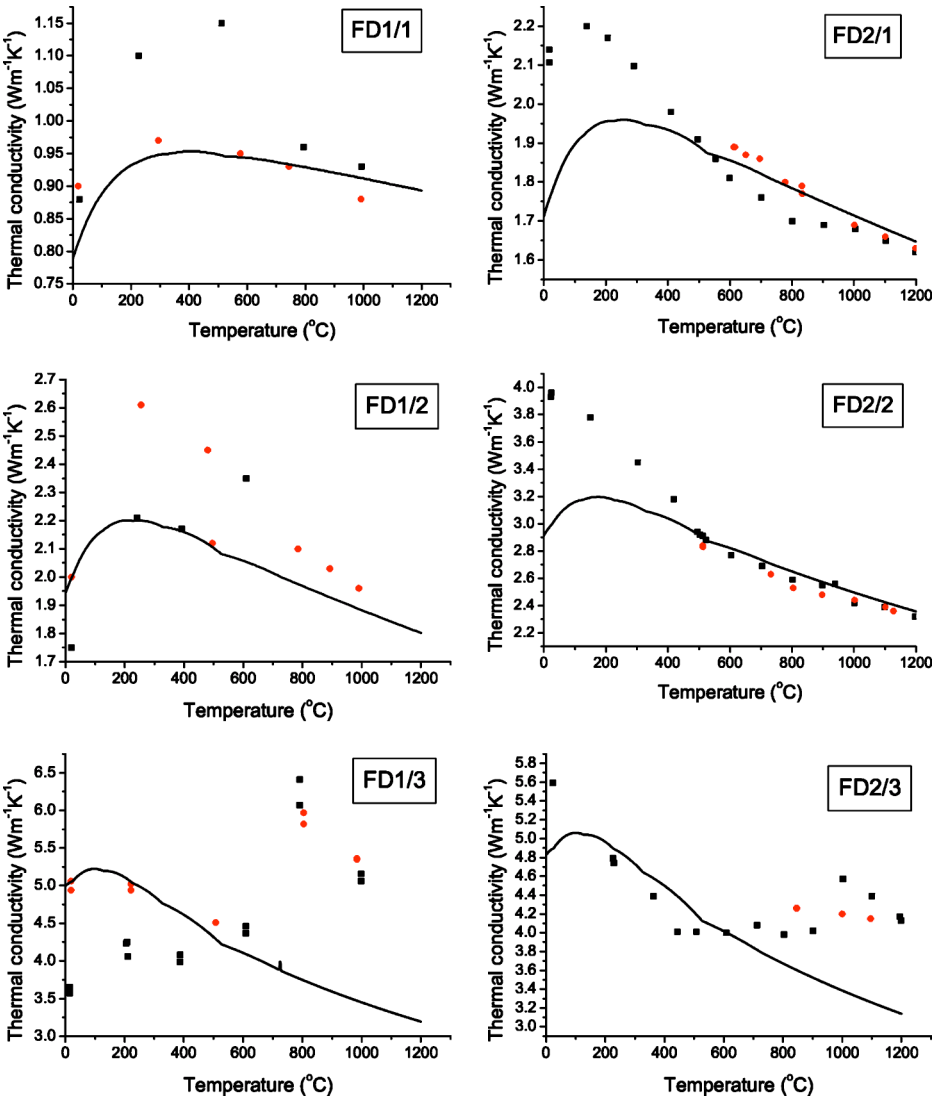

FIG. 3. (Color online) Temperature dependence of TC of the smaples: measured (dots) and calculated (solid line). Different types of the dots indicate the different series of the measurements.

this confirms the approximations of our model. Indeed, as a result of nanostructuring the mean free path of phonons is determined by the grain boundaries, and it is independent of the phonon frequency and the temperature. This is the main reason why the short wavelength phonons, which prevail at high temperatures, are mostly responsible for the heat transport. In the single crystals, on the contrary, the phonon mean free path, which is determined by the phonon-phonon interaction, decreases with the frequency as $l \propto \omega^{-2}$, so that the phonons of any frequency are of equal importance for TC. This enables one to estimate roughly the t value from Eq. (2). The results are close to that of Table I.

Measured values of thermal conductivity as a function of temperature are presented in Fig. 3. We see that theoretical curves as a rule demonstrate more rapid decrease with temperature than observed. This means that the expression Eq. (3) overestimates the influence of the phonon-phonon interaction. Indeed, when obtaining Eq. (3) we had assumed this interaction as independent of scattering at the grain boundaries; we suppose $1/l = 1/l_B + 1/l_{\mathrm{ph}}$, where l is the phonon mean free path, l_B and l_{ph} are the phonon mean free paths relative to scattering at the grain boundaries and the phonon-phonon interaction, respectively. Actually, we have to take into account only the interactions that affect the phonon hopping from one grain into another. Since the in-grain phonon-phonon scattering affects only the density of the phonon states inside the grain, but it does not change the thermal conductivity.

The radiative component alone causes an increase of TC at high temperatures. This follows from Eq. (7), if N_e is independent of temperature. This is of particular importance for specimens of low porosity due to an increase of the effective photon mean free path [Eq. (8)]. We have observed some increase of TC for the specimen FD1/3; however, its value is comparable with the experimental errors.

The grain size dependence of TC following from Eq. (3) is close to that estimated with the Kapitza model[16,17]

$$\kappa_{ph} = \frac{\kappa_i}{1 + \dfrac{\kappa_i}{G_k d}}, \tag{9}$$

where G_k is the Kapitza conductance. Indeed, Eq. (9) results from Eq. (3), if we substitute x by its average value $\overline{x}$. Thus,

$$G_k = \frac{k_B^2 Z t \overline{S} \Phi(\sigma) T_D B(\overline{x})}{3\pi\hbar a^2 d^2}.$$

In particular, at low temperatures when $\kappa_i \gg \kappa_{\mathrm{ph}}$ this expression accepts the form

$$G_k = \frac{k_B^2 Z t \overline{S} \Phi(\sigma) T_D}{3\pi\hbar a^2 d^2} \int_0^{1/\theta} B(x)dx.$$

Apparently G_k is independent of the grain size, if $\overline{S} \propto d^2$; however, it depends on temperature in agreement with Ref. 17. More precisely, temperature dependence of the factor $\int_0^{1/\theta} B(x)dx$ (see Fig. 6 of Ref. 2) has the form of Fig. 6 of Ref. 17, where the temperature dependence of the Kapitza conductance G_k is presented. This allows us to interpret our phenomenological parameter $t \propto G_k$ as the transparency of a grain boundary for the short wavelength phonons.

Strictly speaking, the average value of $\overline{x}$ resulting from the integrand (3) depends on d. Therefore, $B(\overline{x})$ and so the Kapitza conductance G_k also depend on d. This dependence could be significant, if $\kappa_i \lesssim \kappa_{ph}$ at low temperatures $T \lesssim T_D$, when the simple expression (9) could be impracticable.

The parameter $\overline{S}$ determines the influence of the small size pores. Indeed, this value should be equal to d^2 in the absence of pores. If we assume a cubic shape of grains and suppose the pores lie along the cube edges then for the porosity we obtain

$$p = \frac{3\pi}{4}\left(\frac{d-x}{d}\right)^2\left[1 - \frac{4}{9}\left(\frac{d-x}{d}\right)\right],$$

where x is the "neck" size ($\overline{S} = x^2$). For the model of spherical grains such an estimation has been carried out in Ref. 14. The main deviation of both estimations is due to the large size pores, i.e., the pores of about or greater than the grain size. To estimate their influence, we have to remove some resistors from our net, so that their resistivity becomes equal to infinity; this means the absence of the neighbors for some grains due to the large scale porosity. This factor can be related to the cohesion C of each sample, which can be measured experimentally. Cohesion is an average ratio of the number of boundaries grain/pore to the number boundaries grain/grain along some straight line in the TEM pattern. Assuming a homogeneous distribution of the pores, we can estimate the density of the nonremoved resistors in the net as

$$\eta = \frac{C}{2 - C}.$$

Then the expression for TC should be multiplied by η, if $\eta \approx 1$. In the case of large porosity we have to take into account the problem of "dead ends." In the more general case the problem has to be considered with the percolation technique.[7] The resistivity of the net has an increase (and so the TC of our structure has a decrease) at $\eta \simeq 3/(2Z)$, then the expression for TC should be multiplied by $[\eta - 3/(2Z)]$[1.6]. At smaller values of η the short-wavelength phonons becomes localized, and heat transport would occur due to long-wavelength phonons only. Such a situation cannot be realized in porous nanostructures, but it seems to be the case in composite structures where the nanostructure is embedded into some amorphous media.

Our model Eq. (3) considers only the short-wavelength phonon transport. Nevertheless, the long-wavelength phonons, i.e., phonons that wavelength is about or exceeds the grain size $\lambda > d$, also participate in the heat transfer. For a rough estimation of their effect (κ_λ) we suppose that the phonons in each frequency interval within $\omega < \omega_{\mathrm{D}}(a/d)$ make the same contribution to the TC. This is the case of phonon-phonon interaction when the larger number of the phonons with larger frequencies compensates the smaller value of their mean free path.[1] For $T > T_{\mathrm{D}}$ this leads to $\kappa_\lambda \sim \kappa_i(a/d)$. For the smaller temperatures we have to take into account only the phonons with $\hbar\omega < k_{\mathrm{B}}T$, so that $\kappa_\lambda \sim \kappa_i(a/d)(T_{\mathrm{D}}/T)$. There are two possibilities when this value might be important: at low temperatures and in the case of the above-mentioned localization of the short-wavelength phonons.

ACKNOWLEDGMENTS

The authors are indebted to Dr. M. Nygren and Dr. Z. Zhao (University of Stockholm) for sintering of the alumina powders and to Dr. A. Hessler-Wyser (Swiss Federal Institute of Technology, Lausanne) for TEM study. We thank TOP NANO21 (Swiss Commission for Technical Innovations, Project No. 5418.2) for the financial support, and Biakowski SA (France) for the alumina powders.

APPENDIX: PROPAGATION OF ELECTROMAGNETIC WAVES IN A GRANULAR MATERIAL

Consider propagation of the waves in the media with a position dependant dielectric permittivity: $\epsilon(\mathbf{r}) = \varepsilon + \xi(\mathbf{r})$, where $\varepsilon = p\epsilon_1 + (1-p)\epsilon_2$ is the average permittivity, which is independent of $\mathbf{r}$, and the random function $\xi(\mathbf{r})$ is its deviation, $\langle\xi\rangle = 0$; ϵ_1 and ϵ_2 are permittivities of the grains and the surrounded material, and p is concentration of the grains. Angle brackets denote the averaging over the random value ξ. Let $\boldsymbol{E}$ and $\boldsymbol{H}$ be the electrical and magnetic fields of the electromagnetic wave. We can write $\boldsymbol{E} = \boldsymbol{\mathcal{E}} + \boldsymbol{e}$ and $\boldsymbol{H} = \boldsymbol{\mathcal{H}} + \boldsymbol{h}$, where $\boldsymbol{\mathcal{E}}$, $\boldsymbol{\mathcal{H}}$, $\boldsymbol{e}$, and $\boldsymbol{h}$ are the average and fluctuate components of the fields ($\langle\boldsymbol{e}\rangle = \langle\boldsymbol{h}\rangle = 0$).

Suppose different components of the fields fluctuate independently $\langle e_i e_j^*\rangle \propto \delta_{ij}$, then $\langle \boldsymbol{e} \times \boldsymbol{h}^*\rangle \propto \langle \boldsymbol{e} \times (\nabla \times \boldsymbol{e}^*)\rangle = 0$. Therefore, for the averaged Poynting vector we obtain

$$\langle \boldsymbol{S}\rangle = \frac{1}{8\pi}\langle \boldsymbol{\mathcal{E}}(\mathbf{r}) \times \boldsymbol{\mathcal{H}}^*(\mathbf{r})\rangle + \mathrm{c.c.}$$

This means that only the average fields $\boldsymbol{\mathcal{E}}$ and $\boldsymbol{\mathcal{H}}$ determine the energy transfer. To find the effective dielectric permittivity of the material $\tilde{\varepsilon}$ and attenuation of the average fields of the electromagnetic wave γ, we have to write the Maxwell equations for the fields and average them over the random values. This leads to the following equation for the average and fluctuating components:

$$\nabla \times \boldsymbol{\mathcal{E}} = ik_0 \nabla \times \boldsymbol{\mathcal{H}},$$

$$\nabla \times (\nabla \times \boldsymbol{\mathcal{E}}) = k_0^2 \varepsilon \boldsymbol{\mathcal{E}} + k_0^2 \langle \xi(\mathbf{r}) e(\mathbf{r}) \rangle,$$

$$\Delta e + k_0^2 \varepsilon e = \tfrac{1}{\varepsilon} \text{grad div}(\xi \boldsymbol{\mathcal{E}}) + k_0^2 \xi \boldsymbol{\mathcal{E}}. \tag{A1}$$

Here $k_0 = \omega/c$, ω, and c are the wave vector, frequency, and the speed of light in vacuum. Solution of the last equation is

$$e(\mathbf{r}) = \int G(\mathbf{r} - \mathbf{r}')\{\varepsilon^{-1} \text{grad div}[\xi(\mathbf{r}')\boldsymbol{\mathcal{E}}(\mathbf{r}')] + k_0^2 \xi(\mathbf{r}')\boldsymbol{\mathcal{E}}(\mathbf{r}')\} d\mathbf{r}',$$

where the Green's function $G(\mathbf{r}-\mathbf{r}')$ obeys the equation

$$\Delta G + k_0^2 \varepsilon G = 4\pi \delta(\mathbf{r} - \mathbf{r}').$$

Thus, for the average component of the electric field we can write

$$\Delta \boldsymbol{\mathcal{E}} + k_0^2 \varepsilon \boldsymbol{\mathcal{E}} + k_0^2 \boldsymbol{\Pi} = -\frac{1}{\varepsilon} \text{grad div} \boldsymbol{\Pi}, \tag{A2}$$

where

$$\boldsymbol{\Pi}(\mathbf{r}) = \langle \xi(\mathbf{r}) \rangle e(\mathbf{r}) = \int G(\mathbf{r} - \mathbf{r}') \langle \xi(\mathbf{r}) \times \{\varepsilon^{-1} \text{grad div}[\xi(\mathbf{r}')\boldsymbol{\mathcal{E}}(\mathbf{r}')] + k_0^2 \xi(\mathbf{r}')\boldsymbol{\mathcal{E}}(\mathbf{r}')\} \rangle d\mathbf{r}'$$

or

$$\boldsymbol{\Pi}(\mathbf{r}) = \int G(\mathbf{r} - \mathbf{r}')\{\varepsilon^{-1} \text{grad div}[W(\mathbf{r} - \mathbf{r}')\boldsymbol{\mathcal{E}}(\mathbf{r}')] + k_0^2 W(\mathbf{r} - \mathbf{r}')\boldsymbol{\mathcal{E}}(\mathbf{r}')\} d\mathbf{r}', \tag{A3}$$

if we assume a homogeneous distribution of the grains and introduce the correlation function $W(\mathbf{r}-\mathbf{r}') = \langle \xi(\mathbf{r}) \xi(\mathbf{r}') \rangle$. The equality grad div$\boldsymbol{\mathcal{E}} = -$grad div$\boldsymbol{\Pi}/\varepsilon$ has been used when Eq. (A2) was obtained.

Thus, Eq. (A2) is the integral equation with respect to $\boldsymbol{\mathcal{E}}$. To solve it, let us assume $\boldsymbol{\mathcal{E}} = \{\boldsymbol{\mathcal{E}}_x, 00\} e^{ip_z z}$. Then Eq. (A3) accepts the form

$$\boldsymbol{\Pi}(\mathbf{r}) = \Pi_x(\mathbf{r}) = \boldsymbol{\mathcal{E}}_x e^{ip_z z} \int \left[k_0^2 - \frac{(k_z - p_z)^2}{\varepsilon} \right] G(k) \tilde{W}(\mathbf{p} - \mathbf{k}) \frac{d^3k}{(2\pi)^3}, \tag{A4}$$

where $\tilde{W}(k) = \int W(\rho) e^{-i\mathbf{p}\boldsymbol{\rho}} d^3\rho$ is the Fourier transform of the correlation function and $G(k) = (k^2 - \varepsilon k_0^2 - i\delta)^{-1}$ is the Fourier transform of the Green's function.

It is apparent from Eq. (A2) that the real part of $\boldsymbol{\Pi}$ is the effective correction to the permittivity whereas its imaginary part leads to attenuation of the plane wave $\boldsymbol{\mathcal{E}} \exp(i\mathbf{pr})$. If we assume $W(\rho) = \vartheta^2 \exp(-\rho/\mathcal{R})$, where $\vartheta^2 = \langle \xi \rangle^2 = p(1-p)(\epsilon_1 - \epsilon_2)^2$ and $\mathcal{R}$ is the correlation length (approximately this is the mean distance between the pores),[18] then

$$W(k) = \int W(\rho) e^{ik\rho} d^3\rho = \frac{8\pi\vartheta^2\mathcal{R}^3}{(1 + k^2\mathcal{R}^2)^2}.$$

Estimation of (A4) for $k_0\mathcal{R} \ll 1$ leads to the effective permittivity

$$\tilde{\varepsilon} = \varepsilon - \frac{\vartheta^2}{3\varepsilon} + \frac{2}{3} i \vartheta^2 \sqrt{\varepsilon} (k_0\mathcal{R})^3, \tag{A5}$$

so that

$$\gamma = \frac{\vartheta^2}{3} k_0^4 \mathcal{R}^3. \tag{A6}$$

Thus, $\gamma\mathcal{R} \sim (k_0\mathcal{R})^4 \ll 1$. Therefore, only the irregularities which are larger or comparable with the wavelength of the light can affect essentially the radiative part of thermal conductivity. It follows from Eq. (A5) that the effective dielectric permittivity $\tilde{\varepsilon}$ is less than its average value ε. Note, however, that large corrections to ε are beyond the scope of our approximation.

*Electronic address: brag@isp.nsc.ru

[1] P. G. Klemens and M. Gell, Mater. Sci. Eng., A **245**, 143 (1998).
[2] L. Braginsky, N. Lukzen, V. Shklover, and H. Hofmann, Phys. Rev. B **66**, 134203 (2002).
[3] Jie Zou and Alexander Balandin, J. Appl. Phys. **89**, 2932 (2001).
[4] A. Khitin, A. Balandin, J. L. Liu, and K. L. Wang, J. Appl. Phys. **88**, 696 (2000).
[5] Alexander Balandin and Kang L. Wang, J. Appl. Phys. **894**, 6149 (1998); A. Khitin, A. Balandin, J. L. Liu, and K. L. Wang, Superlattices Microstruct. **30**, 1 (2001).
[6] David G. Cahill, Wayne K. Ford, Kenneth E. Goodson, Gerald D. Mahan, Arun Majumdar, Humphrey J. Maris, Roberto Merlin, and Simon R. Phillpot, J. Appl. Phys. **93**, 793 (2003).
[7] B. I. Shklovskii and A. L. Efros, *Electronic Properties of Doped Semiconductors* (Springer-Verlag, Berlin, 1984).
[8] W. J. Parker, R. Jenkins, C. P. Burner, and G. L. Abort, J. Appl. Phys. **32**(9), 1679 (1961).
[9] S. Namba, P. H. Kim, and T. Arai, J. Appl. Phys. **36**(8), 661 (1967).
[10] D. Weaire and L. Phelan, Philos. Mag. Lett. **24**, 107 (1994).
[11] We have not considered the hole contribution to the conductivity because the effective mass of the hole in Al_2O_3 much exceeds that of the electron.
[12] Yong-Nian Xu and W. Y. Ching, Phys. Rev. B **43**, 4461 (1991).
[13] K. Matsunaga, T. Tanaka, T. Yamamoto, and Y. Ikuhara, Phys. Rev. B **68**, 085110 (2003).
[14] V. V. Skorohod, *Rheological Basis of the Theory of Sintering* (Naukova Dumka, Kiev, 1972).
[15] *Alumina as a Ceramic Material*, edited by W. Gitzen (American Ceramic Society, Westerville, Ohio, 1970).
[16] P. L. Kapitza, J. Phys. (Moscow) **4**, 181 (1941).
[17] Ho-Soon Yang, G.-R. Bai, L. J. Thompson, and J. A. Eastman, Acta Mater. **50**, 2309 (2002).
[18] M. V. Berry, Philos. Trans. R. Soc. London, Ser. A **273**, 611 (1973); J. M. Ziman, *Models of Disorder. The Theoretical Physics of Homogeneously Disordered Systems* (Cambridge University Press, Cambridge, 1979).